Faraday Discussions

Accepted Manuscript

This manuscript will be presented and discussed at a forthcoming Faraday Discussion meeting. All delegates can contribute to the discussion which will be included in the final volume.

Register now to attend! Full details of all upcoming meetings: http://rsc.li/fd-upcoming-meetings

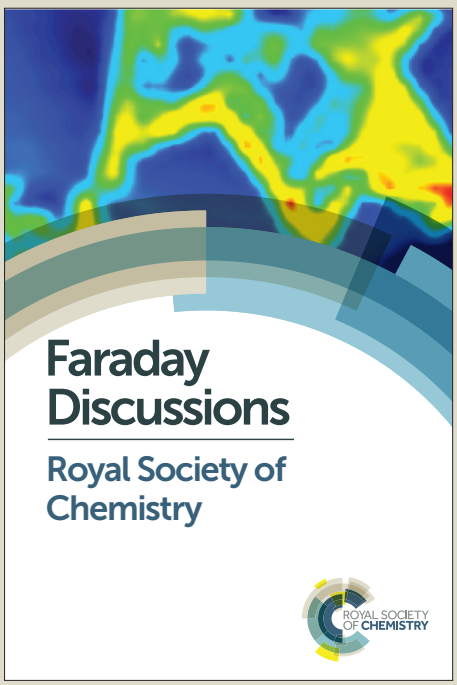

This is an *Accepted Manuscript*, which has been through the Royal Society of Chemistry peer review process and has been accepted for publication.

Accepted Manuscripts are published online shortly after acceptance, before technical editing, formatting and proof reading. Using this free service, authors can make their results available to the community, in citable form, before we publish the edited article. We will replace this *Accepted Manuscript* with the edited and formatted *Advance Article* as soon as it is available.

You can find more information about *Accepted Manuscripts* in the Information for Authors.

Please note that technical editing may introduce minor changes to the text and/or graphics, which may alter content. The journal's standard Terms & Conditions and the Ethical guidelines still apply. In no event shall the Royal Society of Chemistry be held responsible for any errors or omissions in this *Accepted Manuscript* or any consequences arising from the use of any information it contains.

ROYAL SOCIETY OF CHEMISTRY

www.rsc.org/faraday_d

Electrode Kinetics of the NiO Porous Electrode for Oxygen Production in the Molten Carbonate Electrolysis Cell (MCEC)

Lan Hu*, Göran Lindbergh and Carina Lagergren

Applied Electrochemistry, Department of Chemical Engineering and Technology,
KTH Royal Institute of Technology, SE-100 44 Stockholm, Sweden

*Corresponding author. Tel: +46 8 7908244; E-mail: lanhu@kth.se

Abstract

The performance of a molten carbonate electrolysis cell (MCEC) is to a great extent determined by the anode, i.e. the oxygen production reaction on the porous NiO electrode. In this study stationary polarization curves for the NiO electrode were measured under varying gas compositions and temperatures. The exchange current densities were calculated numerically from the slopes at low overpotential. Positive dependence on the exchange current density was found for the partial pressure of oxygen. When the temperature increased in the range of 600–650 °C, the reaction order of oxygen decreased from 0.97 to 0.80. However, there were two different cases for the partial pressure dependency of carbon dioxide within this temperature range: positive values, 0.09–0.30, at lower CO_2 concentration, while the reaction order changed to negative values, -0.26–0.01, with increasing CO_2 content. A comparison of data obtained theoretically indicates that the oxygen-producing reaction in MCEC could be reasonably satisfied by the reverse of oxygen reduction by the oxygen mechanism I, an n=4 electron reaction, assuming a low coverage of oxygen ions at high CO_2 content and an intermediate coverage for a low CO_2 concentration.

Introduction

There is a growing interest in high-temperature electrolysis cell technology today for producing hydrogen and/or syngas, since these fuels are considered important in future energy systems. Electrolysis in molten carbonate salts at high temperature (typically 650 °C) is a promising option, especially when combining with renewable electricity resources such as wind power and/or solar energy. Some researchers have evidenced the possibility of electrolysis in molten carbonates but mainly by converting CO_2 into CO [1-4]. But most experiments were performed on flag electrodes, which are different from porous electrodes as concerns electrode surface and mass-transport properties. Our previous study [5] has shown that it is feasible to run the molten carbonate fuel cell reversibly with conventional Ni-based porous electrodes at 650 °C. Lower polarization loss has been found for the electrolysis cell than for the fuel cell, mainly due to the NiO electrode performing much better as anode in MCEC mode [5]. The activity of the NiO electrode gives the dominant contribution to the performance of the cell, regardless of fuel cell or electrolyzer operation. Thus it is essential to elucidate the kinetics on the NiO porous electrode for oxygen reduction in the fuel cell, as well as for oxygen production in the electrolysis cell.

However, the kinetics and reaction mechanism on the NiO porous electrode as an anode for oxygen production in MCEC mode are still unknown. Then a feasible path is to understand whether the reversed process of oxygen reduction takes place on the NiO electrode or whether there are some other electrochemical/chemical reaction pathways in electrolysis operation. Several reaction mechanisms for the oxygen reduction reaction in the fuel cell mode have been discussed in the literature [6-12], see Table 1. The corresponding reaction orders of oxygen and carbon dioxide for these five mechanisms have been reported by Makkus [13] for varying rate-determining steps (rds). According to Appleby and Nicholson [6-8], in pure lithium and lithium rich melts the peroxide (O_2^{2-}) mechanism was suggested, while the superoxide (O_2^-) path seemed to be involved in sodium and potassium-rich melts for oxygen reduction. Dunks and Stelman [9] and Takahashi [10] proposed the mechanism based on peroxycarbonate (CO_4^{2-}) ion. Kunz et al. [11] suggested oxygen mechanism I to evaluate the concept of the homogeneous/agglomerate model. Makkus et al. [12] discussed oxygen mechanism II for the thin-film model. All proposed mechanisms consist of two or more single electron transfer reactions. All these five reaction mechanisms show the same final recombination reaction step

$$O^{2-} + CO_2 \rightleftharpoons CO_3^{2-} \quad (1)$$

Kunz and Murphy [14], Lu and Selman [15], and Peelen et al. [16] suggested that this recombination reaction is possibly the rate-determining step in porous electrodes under MCFC conditions, due to the low reaction rate.

Table 1 Reaction mechanisms for oxygen reduction reported in the literature [6-12].

The peroxide mechanism: n=2
$O_2 + 2CO_3^{2-} \rightleftharpoons 2O_2^{2-} + 2CO_2$
$O_2^{2-} + e^- \rightleftharpoons O^{2-} + (O^-)$
$(O^-) + e^- \rightleftharpoons O^{2-}$
$O^{2-} + CO_2 \rightleftharpoons CO_3^{2-}$
The superoxide mechanism: n=3
$O_2 + 2CO_3^{2-} \rightleftharpoons O_2^{2-} + 2CO_2$
$O_2 + O_2^{2-} \rightleftharpoons 2O_2^-$
$O_2^- + e^- \rightleftharpoons O_2^{2-}$
$O_2^{2-} + e^- \rightleftharpoons O^{2-} + (O^-)$
$(O^-) + e^- \rightleftharpoons O^{2-}$
$O^{2-} + CO_2 \rightleftharpoons CO_3^{2-}$
The peroxycarbonate mechanism: n=2
$O_2 + 2CO_3^{2-} \rightleftharpoons 2CO_4^{2-}$
$CO_4^{2-} + e^- \rightleftharpoons CO_3^{2-} + (O^-)$
$(O^-) + e^- \rightleftharpoons O^{2-}$
$O^{2-} + CO_2 \rightleftharpoons CO_3^{2-}$
Oxygen mechanism I: n=4
$O_2 + e^- \rightleftharpoons O_2^-$
$O_2^- + e^- \rightleftharpoons O_2^{2-}$
$O_2^{2-} + e^- \rightleftharpoons O^{2-} + (O^-)$
$(O^-) + e^- \rightleftharpoons O^{2-}$
$O^{2-} + CO_2 \rightleftharpoons CO_3^{2-}$
Oxygen mechanism II: n=2
$O_2 \rightleftharpoons 2O$
$O + e^- \rightleftharpoons O^-$
$O^- + e^- \rightleftharpoons O^{2-}$
$O^{2-} + CO_2 \rightleftharpoons CO_3^{2-}$

In MCEC mode the main electrochemical reaction taking place on the NiO porous electrode for oxygen production is electrolysis of the carbonate ion (CO_3^{2-})

$$CO_3^{2-} \rightleftharpoons \frac{1}{2}O_2 + CO_2 + 2e^- \quad (2)$$

Sugiura et al. [17] suggested separation of CO_2 in a molten carbonate fuel cell (MCFC) device. One of the options suggested was to use reaction (2) as anode reaction in the device.

This paper aims to study the kinetics and reaction mechanism of the NiO porous electrode for oxygen production in MCEC operation. For this purpose the general procedure is to determine the reaction orders of oxygen and carbon dioxide. Thus the steady-state polarization data are investigated for varying gas compositions and operating temperatures. The exchange current densities, differing with the concentration of the electroactive species and the temperature, are calculated numerically from the slopes of the polarization curves at low overpotential. Based on this, the partial pressure dependencies of oxygen and carbon dioxide could be evaluated. Meanwhile, a possible reaction mechanism is proposed for oxygen production on the NiO porous electrode in MCEC mode.

Experimental

The cell set-up used in this study is identical to that described in a previous study [5]. Experimental data were obtained from the laboratory cell unit with a geometrical area of 3 cm^2, where the cell components are provided by Ansaldo Fuel Cells in Italy. The cell has a porous Ni, oxidized and lithiated in situ as anode, and a porous Ni-Cr alloy as cathode. The electrodes are separated by a porous $LiAlO_2$ matrix, which also supports the electrolyte, a eutectic mixture of 62/38 mol% Li_2CO_3/K_2CO_3. The current collectors used on the NiO and Ni electrode side are made of stainless steel SS316 and nickel, respectively. Two probes of the current collector are each separately measuring the current and the potential. Two reference electrodes, consisting of Au wires in equilibrium with a gas mixture of 33/67% O_2/CO_2, are placed in separate chambers filled with the same electrolyte as in the cell. These chambers are connected to the cell through a capillary with a gold plug.

The cell is operated at three different temperatures, 600, 625 and 650 °C. The inlet fuel gas mixture consisting of 25/25/25/25% $H_2/CO_2/H_2O/N_2$ is introduced to the Ni electrode. The concentration of H_2O in the fuel gas is controlled by the temperature of the water in the humidifier, 65 °C. The different gas mixtures of $O_2/CO_2/N_2$ for the NiO electrode are shown in Table 2. The concentrations of oxygen and carbon dioxide are varied separately in group 1 and group 2. The O_2 and CO_2 partial pressures increase in the ranges of 1.5–30% and 2.5–40%, respectively. In order to reduce the effect of mass-transfer limitations in the gaseous phase, the flow rates of inlet gases for the NiO porous electrode are held at as high as approximately 250 $ml \cdot min^{-1}$. The gas flow rate for the Ni electrode is also about 250 $ml \cdot min^{-1}$, while the reference gas has a flow rate of 20 $ml \cdot min^{-1}$. All the gases used in the experiments are certified gas mixtures from AGA Gas AB, Sweden.

Table 2 The inlet gas compositions, by percent.

Gas No.	O_2/%	CO_2/%	N_2/%
(1) changing O_2			
1.1	1.5	30	68.5
1.2	2.5	30	67.5
1.3	5	30	65
1.4	10	30	60
1.5*	15	30	55
1.6	20	30	50
1.7	25	30	45
1.8	30	30	40
(2) changing CO_2			
2.1	15	2.5	82.5
2.2	15	5	80
2.3	15	10	75
2.4	15	15	70
2.5	15	20	65
2.6	15	25	60
2.7*	15	30	55
2.8	15	35	50
2.9	15	40	45

*the standard inlet gas, 15/30/55% $O_2/CO_2/N_2$

The polarization curves are measured using a Solartron Interface SI1287 supported by CorrWare software. The current-interrupt technique is used to separate the ohmic loss from other types of polarization. In this paper, the negative current density refers to the electrolysis mode, shown in the figures below.

Theory

Elucidating the kinetics and mechanism of reaction (2) is generally done by determining the partial pressure dependencies of oxygen and carbon dioxide. The same method was used to understand the hydrogen production on the cathode side, the Ni electrode [18]. When analyzing kinetic data it is important to consider the current distribution along the depth of the NiO electrode due to its porous characteristics [19]. The current distribution is determined by the combination of the electrode intrinsic activity, its specific surface area, the effective diffusion path lengths of electroactive species, and the effective conductivities of the electrolyte and electrode. In the present study the polarization data are analyzed only at a low overpotential range, where the electrode is assumed to be mainly under

charge-transfer limitation and the influence of mass-transfer limitation is negligible. According to Lagergren and Simonsson [20], in order to take the current distribution into account when analyzing data, the expression for the total polarization resistance is

$$\frac{d\eta}{di} = \frac{L}{\kappa_1+\kappa_2} + \frac{L}{\sqrt{a}} \cdot \frac{1}{\kappa_1+\kappa_2} \cdot \left[\frac{2}{\sinh\sqrt{a}} + \left(\frac{\kappa_1}{\kappa_2} + \frac{\kappa_2}{\kappa_1}\right)\coth\sqrt{a}\right] \quad (3)$$

where

$$a = \frac{nFL^2Si_0}{RT}\left(\frac{1}{\kappa_1} + \frac{1}{\kappa_2}\right) \quad (4)$$

L is the electrode thickness, κ_1 and κ_2 are the effective conductivities in the electrode and electrolyte phases, respectively. S is the exterior agglomerate surface area.

There are two limiting cases of Eq. (3), in which a approaches either zero or infinity. These two cases refer to uniform and uneven current distribution, respectively.

According to Eq. (3), the ohmic loss, $\frac{\mathrm{L}}{\kappa_1+\kappa_2}$, due to the finite conductivities of the electrolyte and the electrodes, is included in the total polarization resistance. In this study the current-interrupt technique is used to correct the iR drop, and therefore the experimentally obtained polarization data does not contain the ohmic contribution.

The partial pressure dependencies of oxygen and carbon dioxide can be expressed as

$$i_0 = i_0^0\left(p_{O_2}\right)^x\left(p_{CO_2}\right)^y \quad (5)$$

where i_0^0 is the standard exchange current density, and x and y denote the reaction orders of oxygen and carbon dioxide, respectively.

Results and Discussion

In Fig. 1 the iR-corrected polarization curves for different gas compositions at 650 °C are shown. The blue curves in the figure correspond to the performance of the NiO electrode with the standard inlet gas of 15/30/55% $O_2/CO_2/N_2$ in the electrolysis operation. The red symbols refer to the gases with lower content than the standard level when changing O_2 and CO_2 partial pressures separately, while the green symbols refer to the gases with higher concentration. In Fig. 1(a) the polarization loss of the NiO electrode decreases gradually when increasing the concentration of O_2 from 1.5 to 30%. The polarization curves show a tendency to bend downward at high current densities, and under lower O_2 content that bending is observed even at the low current density. It seems that mass-transfer limitation does not take place at high current density, otherwise the curves would be bending upward. When

increasing CO_2 content in the range of 2.5–20%, the activity of the NiO electrode shows a slow improvement in oxygen production at 650 °C, as shown in Fig. 1(b). But with the increase of CO_2 from 20 to 40% only a very small impact on the polarization loss of the NiO electrode is observed also at high current density.

In order to make a more thorough analysis of the polarization data, the electrochemical performance of the NiO electrode was investigated within a low overpotential range, < 45mV, at 600-650 °C. Varying the concentration of O_2 within the range of 1.5–30% gives the quasi-linear characteristic of the iR-corrected curves at all measured temperatures visualized in Fig. 2. Increase of O_2 content improves the NiO electrode for oxygen production in the electrolysis operation. However, the impact of CO_2 concentration on the polarization performance of the NiO electrode is strongly dependent on temperature, as shown in Fig. 3. At 600 °C, increasing CO_2 from 2.5 to 10% gives only a small improvement of the performance of the NiO electrode, while a contrary tendency of slowly poorer behavior of the electrode takes place when increasing CO_2 to higher concentration (40%). In Fig. 3(b) the polarization loss of the NiO electrode decreases gradually as the CO_2 concentration rises from 2.5 to 15%, and then it shows a very small increasing trend of the electrode polarization with increasing CO_2 in the range of 15–40% at 625 °C. When reaching 650 °C the NiO electrode has an improved activity for oxygen production when containing 2.5–20% CO_2, and the electrode performance remains almost stable within the partial pressure range of 20–40%, seen in Fig. 3(c). The carbon dioxide content affecting the performance of the NiO electrode for oxygen production varies with the temperature. It is assumed that the electrode in this low overpotential range is under kinetic control as it is not necessary to take mass-transfer limitations in consideration. All the measured polarization curves are quasi-linear, from the slopes of these curves the polarization resistances, $\frac{d\eta}{di}$, could thus be evaluated by linear regression analysis.

The exchange current density for each gas composition and temperature could be obtained by solving Eq. (3). Parameter values used for solving Eq. (3) are listed in Table 3. It is assumed that the NiO electrode has a pseudo-homogeneous structure and that the electrode reaction takes place mainly at the exterior surface of the agglomerates [19]. Assuming that the agglomerates are spherical and have a radius of 5 μm, the external agglomerate area, S, is estimated to be $3 \cdot 10^5$ m^{-1} [19]. The effective conductivity of the porous NiO electrode is in the order of 1000 $S \cdot m^{-1}$ [20, 21]. The effective conductivity in the pore electrolyte was measured to be 0.9–2.2 $S \cdot m^{-1}$ at 650 °C [22]. Thus in this work the effective electrolyte conductivity at 650 °C is set to 2.0 $S \cdot m^{-1}$, from which the values of 1.7 $S \cdot m^{-1}$ and 1.8 $S \cdot m^{-1}$ were calculated at 600 and 625 °C, respectively, using the Arrhenius equation [23]. The exchange current density i_0 for the standard inlet gas, 15/30/55% O_2/CO_2 /N_2 (1.5* and 2.7* in Table 4), shows an increase from 4.0 to 22.7 $A \cdot m^{-2}$ when the temperature is raised from 600 to 650 °C.

The value of i_0 for oxygen production in the electrolysis cell is in the same order of magnitude as that for oxygen reduction on the NiO porous electrode in fuel cell mode (22.4 A·m^{-2} at 650 °C) [19].

Table 3 Parameter values used when solving Eq. (3)

		600 °C	625 °C	650 °C
L	0.6 mm			
r	5 μm			
S	$3 \cdot 10^5$ m^{-1}			
n	4			
κ_1	1000 S·m^{-1}			
κ_2		1.7 S·m^{-1}	1.8 S·m^{-1}	2.0 S·m^{-1}

A striking feature of Table 4 is that the exchange current density increases with the oxygen partial pressure when the NiO electrode is used as anode in MCEC mode. The values are in the range of 0.5–8.6, 1.9–25.0 and 3.8–41.4 A·m^{-2} at 600, 625 and 650 °C, respectively. However, concerning the carbon dioxide partial pressure the exchange current density should be analyzed at low content and at higher concentration. For example, the exchange current density increases slightly from 5.0 to 5.7 A·m^{-2} in the range 2.5–10% CO_2 at 600 °C. The value shows a slow decrease to 4.1 A·m^{-2} as the CO_2 concentration reaches 40%. The content of carbon dioxide affects the exchange current density differently for different operating temperatures, in correspondence with the results of the polarization data discussed above. When going to 625 °C, at CO_2 partial pressures of 2.5–15% the exchange current density increases from 8.1 to 12.4 A·m^{-2}, then it presents quite a small reducing interval of 12.4–11.6 A·m^{-2} when containing 15–40% CO_2. As the cell temperature goes to 650 °C, the values of i_0 increases from 12.5 to 22.8 A·m^{-2} with increasing CO_2 concentration from 2.5 to 20%, but then the data remain almost stable within the CO_2 interval of 20–40%. The exchange current density is not as strongly affected by the partial pressure of carbon dioxide as by that of oxygen. This indicates that carbon dioxide may have smaller impact on the charge-transfer polarization of the electrode, since the exchange current density reflects the rate of the charge transfer.

Table 4 Experimentally obtained exchange current densities at different gas compositions and temperatures.

Gas No.	i_0 /A·m^{-2} 600 °C	i_0 /A·m^{-2} 625 °C	i_0 /A·m^{-2} 650 °C
(1) changing O_2			
1.1	0.5	1.9	3.8
1.2	0.8	2.6	5.4
1.3	1.3	4.6	8.9
1.4	2.6	7.9	15.4
1.5*	4.0	12.0	21.6
1.6	5.9	16.5	29.2
1.7	7.3	20.8	35.2
1.8	8.6	25.0	41.4
(2) changing CO_2			
2.1	5.0	8.1	12.5
2.2	5.4	9.7	15.0
2.3	5.7	11.8	19.7
2.4	5.5	12.4	21.4
2.5	5.1	12.4	22.8
2.6	4.6	12.2	22.6
2.7*	4.2	11.9	22.7
2.8	4.2	11.9	23.2
2.9	4.1	11.6	22.7

The reaction orders of oxygen and carbon dioxide at 600–650 °C are determined in Figs. 4–5. The linear regression results show that the oxygen partial pressure dependency decreases from 0.97 to 0.80 in the temperature interval 600–650 °C. However, the dependency of exchange current densities on carbon dioxide partial pressure shows two cases in Fig. 5. At lower CO_2 concentration the reaction order of carbon dioxide gives positive values at all measured temperatures, which alters to negative when increasing the CO_2 content. Specifically, at 600 °C the reaction order of carbon dioxide is 0.09 within the CO_2 content range of 2.5–10%, and becomes negative, -0.26, when containing 10–40% CO_2. In contrast to oxygen, the carbon dioxide partial pressure dependency increases with temperature. When containing 2.5–15% CO_2 at 625 °C the value of the reaction order is 0.25, becoming -0.07 within the concentration range of 15–40% CO_2. When reaching 650 °C the reaction order increases to 0.30 when containing 2.5–20% CO_2. The value changes to 0.01 when increasing the CO_2 concentration to 40%. Thus, within all the measured temperatures from 600 to 650 °C, for a low concentration of CO_2, Eq. (5) can be expressed as

$$i_0 = i_0^0 \left(p_{O_2}\right)^{0.97-0.80} \left(p_{CO_2}\right)^{0.09-0.30} \quad (6)$$

and at a high CO_2 content it could be expressed as

$$i_0 = i_0^0 \left(p_{O_2}\right)^{0.97-0.80} \left(p_{CO_2}\right)^{-0.26-0.01} \quad (7)$$

As discussed above, the partial pressure dependencies obtained in this study are remarkably higher for oxygen than for carbon dioxide. The following reaction paths could probably be the mechanism for the oxygen production reaction in a molten carbonate electrolysis cell, on the basis of the reversed process of oxygen reduction in fuel cell operation (oxygen mechanism I) proposed by Kunz et al. [11].

$$CO_3^{2-} \rightleftharpoons O^{2-} + CO_2 \quad (8)$$

$$O^{2-} \rightleftharpoons (O^-) + e^- \quad (9)$$

$$O^{2-} + (O^-) \rightleftharpoons O_2^{2-} + e^- \quad (10)$$

$$O_2^{2-} \rightleftharpoons O_2^- + e^- \quad (11)$$

$$O_2^- \rightleftharpoons O_2 + e^- \quad \text{rds} \quad (12)$$

It is assumed that (i) reaction (12) of oxygen evolution is the rate-determining step; and (ii) there is a low coverage of oxide ion. Assuming the symmetry factor $\beta = 0.5$ for rate-determining step, the theoretical dependency of i_0 on the gas partial pressure is calculated in detail in Appendix and shown as

$$i_0 = i_0^0 \left(p_{O_2}\right)^{0.875} \left(p_{CO_2}\right)^{-0.25} \quad (13)$$

The theoretical reaction order is 0.875 for oxygen, satisfying well the oxygen partial pressure dependency (0.97–0.80) determined from the experimental data. The theoretical value of -0.25 for carbon dioxide could reasonably fit the reaction order at the high CO_2 concentration, as shown in Eq. (7). But it does not show agreement with the positive dependence at a low CO_2 content. If assuming the oxygen production as the reversed process of oxygen reduction in molten carbonate salts, the theoretical partial pressure dependencies for oxygen and carbon dioxide would be the same in both the fuel cell and the electrolyzer operations. Makkus [13] reported the values of the reaction order for all the reaction mechanisms for oxygen reduction mentioned in Table 1. According to Makkus, the exchange current density with a high coverage of O^{2-} can be expressed as

$$i_0 = i_0^0 \left(p_{O_2}\right)^{0.875} \left(p_{CO_2}\right)^{0.75} \quad (14)$$

The partial pressure dependency of carbon dioxide, y, could be affected by the chemical decomposition of CO_3^{2-} producing O^{2-} and CO_2. For example, the reaction order is stable at 0.875 for

oxygen and the value changes from negative (-0.25) to positive (0.75) for carbon dioxide when containing a high coverage of O^{2-}, see Eq. (14). Lowering the carbon dioxide partial pressure, it makes sense from the perspective of chemical kinetics that the homogeneous reaction ($CO_3^{2-} \rightleftharpoons O^{2-} + CO_2$) will progress to produce the oxide ion. However, the theoretical value of 0.75 is still much higher than the experimental result (0.09–0.30), which indicates that reaction steps (8)–(12) with an intermediate coverage of O^{2-} could constitute a possible mechanism for oxygen production on the NiO porous electrode at a low CO_2 concentration.

The activation energy for the NiO electrode could be calculated by the Arrhenius' equation, see Table 5.

$$E_a = -2.303R\frac{d(\log i_0)}{d(1/T)} \quad (15)$$

For the NiO electrode for oxygen production in MCEC mode with the standard gas, 15/30/55% $O_2/CO_2/N_2$, the value of the activation energy is 226 $\pm$ 1 kJ·mol^{-1}, which is in the same range as for oxygen reduction in fuel cell operation [24]. The calculated activation energy lies between 278 and 211 kJ·mol^{-1} when increasing the O_2 concentration from 1.5 to 30%, but it increases from 124 to 229 kJ·mol^{-1} when varying the CO_2 content from 2.5 to 40%. Gases of low O_2 partial pressure, e.g. 1.5–10% O_2, exhibit much larger activation energy than those with low CO_2 partial pressure, which means that oxygen appears to have a stronger effect on charge-transfer limitation. That is also evidenced by the higher values of reaction order obtained for oxygen compared to carbon dioxide. As the activation energy is a clue to determine the rate-determining process [25], it is probable that the NiO electrode is under mixed control at a quite low CO_2 concentration, and is then limited by charge transfer at high CO_2 concentration. This confirms that at low CO_2 partial pressure the reaction ($CO_3^{2-} \rightleftharpoons O^{2-} + CO_2$) plays an important role in oxygen production in MCEC mode.

Table 5 Calculation of the activation energy for the NiO electrode at different gas compositions.

Gas No.	O_2/%	CO_2/%	N_2/%	Ea/kJ·mol^{-1}
(1) changing O_2				
1.1	1.5	30	68.5	278.3
1.2	2.5	30	67.5	258.5
1.3	5	30	65	254.3
1.4	10	30	60	238.7
1.5*	15	30	55	225.1
1.6	20	30	50	214.7
1.7	25	30	45	211.1
1.8	30	30	40	211.2
(2) changing CO_2				
2.1	15	2.5	82.5	123.6
2.2	15	5	80	138.3
2.3	15	10	75	167.6
2.4	15	15	70	183.5
2.5	15	20	65	202.6
2.6	15	25	60	214.4
2.7*	15	30	55	226.5
2.8	15	35	50	229.0
2.9	15	40	45	229.3

Conclusions

Stationary polarization data have been studied for the NiO electrode, as anode in an electrolyzer, under varying gas compositions and temperatures. The slopes of the polarization curves at a low overpotential range were analyzed, assuming the electrode to be under kinetic control.

The partial pressure dependencies on the exchange current density lie between 0.97 and 0.80 for oxygen in the temperature interval 600–650°C. There are two cases for the reaction order of carbon dioxide, positive values of 0.09–0.30 at a low CO_2 concentration and then negative dependence (-0.26–0.01) with high CO_2 content.

The reverse process of oxygen reduction in MCFC operation, based on oxygen mechanism I, was found to suitably describe oxygen production in the electrolyzer. The theoretical reaction orders were 0.875 for oxygen, and -0.25 for carbon dioxide under the assumption of a low coverage of the oxide ion. Due to the reaction ($CO_3^{2-} \rightleftharpoons O^{2-} + CO_2$), the coverage of O^{2-} is dependent on the carbon dioxide concentration. For a high coverage of O^{2-}, the theoretical dependency changed to 0.75 for CO_2. Thus, according to this study, an intermediate coverage of oxide ion might be achieved at a low CO_2 content.

The activation energy of the NiO porous electrode for oxygen production lies between 278 and 211 kJ·mol^{-1} for increasing O_2 content. In contrast, the values were in the rising range of 124-229 kJ·mol^{-1} when increasing the CO_2 concentration. This indicates that the NiO electrode for oxygen production is generally under charge-transfer limitation, except at a very low CO_2 partial pressure when it was under mixed control.

Acknowledgement

The financial support of the China Scholarship Council (CSC) is appreciated. The cell components were provided by Ansaldo Fuel Cells in Italy.

APPENDIX

Determination of Reaction Order

The reaction mechanism for oxygen production in a molten carbonate electrolysis cell follows

$$CO_3^{2-} \underset{k_{1c}}{\overset{k_{1a}}{\rightleftarrows}} O^{2-} + CO_2 \quad \text{(A-1)}$$

$$O^{2-} \underset{k_{2c}}{\overset{k_{2a}}{\rightleftarrows}} (O^-) + e^- \quad \text{(A-2)}$$

$$O^{2-} + (O^-) \underset{k_{3c}}{\overset{k_{3a}}{\rightleftarrows}} O_2^{2-} + e^- \quad \text{(A-3)}$$

$$O_2^{2-} \underset{k_{4c}}{\overset{k_{4a}}{\rightleftarrows}} O_2^- + e^- \quad \text{(A-4)}$$

$$O_2^- \underset{k_{5c}}{\overset{k_{5a}}{\rightleftarrows}} O_2 + e^- \quad \text{rds} \quad \text{(A-5)}$$

For this mechanism it is assumed that (i) reaction (A-5) is the rate-determining step; and (ii) there is a low coverage of oxide ion.

At equilibrium, reaction (A-1) can be written

$$k_{1a}(1-\theta)C_{CO_3^{2-}} = k_{1c}\theta C_{CO_2} \quad \text{(A-6)}$$

where θ is the coverage of the oxide ion (O^{2-}).

Assuming a low coverage of O^{2-}, $(1-\theta)\sim 1$. From Eq. (A-6) the fraction of θ is

$$\theta = \frac{k_{1a}}{k_{1c}} \cdot \frac{C_{CO_3^{2-}}}{C_{CO_2}} \tag{A-7}$$

The net current from reaction (A-2) is

$$i_2 = F\left\{k_{2a}\theta e^{\beta_2 FE/RT} - k_{2c}(1-\theta)C_{(O^-)}e^{-(1-\beta_2)FE/RT}\right\} \tag{A-8}$$

E is the potential difference between the electrode and the electrolyte. At equilibrium, when $i_2 = 0$

$$C_{(O^-)} = \frac{k_{1a}}{k_{1c}} \cdot \frac{k_{2a}}{k_{2c}} \cdot \frac{C_{CO_3^{2-}}}{C_{CO_2}} e^{FE/RT} \tag{A-9}$$

For reaction (A-3) the net current is

$$i_3 = F\left\{k_{3a}\theta C_{(O^-)}e^{\beta_3 FE/RT} - k_{3c}(1-\theta)C_{O_2^{2-}}e^{-(1-\beta_3)FE/RT}\right\} \tag{A-10}$$

When $i_3 = 0$ at equilibrium,

$$C_{O_2^{2-}} = \left(\frac{k_{1a}}{k_{1c}}\right)^2 \cdot \frac{k_{2a}}{k_{2c}} \cdot \frac{k_{3a}}{k_{3c}} \cdot \left(\frac{C_{CO_3^{2-}}}{C_{CO_2}}\right)^2 e^{2FE/RT} \tag{A-11}$$

The net current for reaction (A-4) is

$$i_4 = F\left\{k_{4a}C_{O_2^{2-}}e^{\beta_4 FE/RT} - k_{4c}C_{O_2^-}e^{-(1-\beta_4)FE/RT}\right\} \tag{A-12}$$

At equilibrium, when $i_4 = 0$

$$C_{O_2^-} = \left(\frac{k_{1a}}{k_{1c}}\right)^2 \cdot \frac{k_{2a}}{k_{2c}} \cdot \frac{k_{3a}}{k_{3c}} \cdot \frac{k_{4a}}{k_{4c}} \cdot \left(\frac{C_{CO_3^{2-}}}{C_{CO_2}}\right)^2 e^{3FE/RT} \tag{A-13}$$

For reaction (A-5) the net current is

$$i_5 = F\left\{k_{5a}C_{O_2^-}e^{\beta_5 FE/RT} - k_{5c}C_{O_2}e^{-(1-\beta_5)FE/RT}\right\} \tag{A-14}$$

Reaction (A-5) is assumed to be the rate-determining step, the equilibrium expression of Eq. (A-14) for the equilibrium potential E^0 upon substitution for $C_{O_2^-}$ from Eq. (A-13)

$$e^{FE^0/RT} = \left[\left(\frac{k_{1c}}{k_{1a}}\right)^2 \cdot \frac{k_{2c}}{k_{2a}} \cdot \frac{k_{3c}}{k_{3a}} \cdot \frac{k_{4c}}{k_{4a}} \cdot \frac{k_{5c}}{k_{5a}} \cdot \left(\frac{C_{CO_2}}{C_{CO_3^{2-}}}\right)^2 \cdot C_{O_2}\right]^{\frac{1}{4}} \tag{A-15}$$

Replacing $E = E^0 + \eta$, where η is the overpotential, in Eq. (A-14), the following can be obtained

$$i_5 = F\left\{k_{5a}\left[\left(\frac{k_{1a}}{k_{1c}}\right)^{\frac{1-\beta_5}{2}}\left(\frac{k_{2a}}{k_{2c}} \cdot \frac{k_{3a}}{k_{3c}} \cdot \frac{k_{4a}}{k_{4c}}\right)^{\frac{1-\beta_5}{4}}\left(\frac{k_{5a}}{k_{5c}}\right)^{-\frac{3+\beta_5}{4}} C_{CO_3^{2-}}{}^{\frac{1-\beta_5}{2}}\right] \cdot C_{O_2}{}^{\frac{3+\beta_5}{4}} \cdot C_{CO_2}{}^{\frac{\beta_5-1}{2}} \cdot e^{(3+\beta_5)F\eta/RT} - k_{5c}\left[\left(\frac{k_{1a}}{k_{1c}}\right)^{\frac{1-\beta_5}{2}}\left(\frac{k_{2a}}{k_{2c}} \cdot \frac{k_{3a}}{k_{3c}} \cdot \frac{k_{4a}}{k_{4c}}\right)^{\frac{1-\beta_5}{4}}\left(\frac{k_{5a}}{k_{5c}}\right)^{\frac{1-\beta_5}{4}} C_{CO_3^{2-}}{}^{\frac{1-\beta_5}{2}}\right] \cdot C_{O_2}{}^{\frac{3+\beta_5}{4}} \cdot C_{CO_2}{}^{\frac{\beta_5-1}{2}} \cdot e^{-(1-\beta_5)F\eta/RT}\right\} \tag{A-16}$$

Eq. (23) may be compared with the general relationship for activation polarization according to the Bulter-Volmer equation

$$i = i_0\left[e^{\alpha_A \eta F/RT} - e^{-\alpha_C \eta F/RT}\right] \quad \text{(A-17)}$$

The exchange current density may be written

$$i_0 = i_0^0\left(C_{O_2}\right)^{\frac{3+\beta_5}{4}}\left(C_{CO_2}\right)^{\frac{\beta_5-1}{2}} \quad \text{(A-18)}$$

where $i_0^0 = \left(\frac{k_{1a}}{k_{1c}}\right)^{\frac{1-\beta_5}{2}}\left(\frac{k_{2a}}{k_{2c}}\cdot\frac{k_{3a}}{k_{3c}}\cdot\frac{k_{4a}}{k_{4c}}\right)^{\frac{1-\beta_5}{4}}\frac{(k_{5a})^{\frac{1-\beta_5}{4}}}{(k_{5c})^{-\frac{3+\beta_5}{4}}}C_{CO_3^{2-}}^{\frac{1-\beta_5}{2}}$ (A-19)

We obtain

$\alpha_A = 3 + \beta_5$, assuming the symmetry factor $\beta_5 = 0.5$, so $\alpha_A = 3.5$

and $\alpha_C = 1 - \beta_5 = 0.5$

The dependency of i_0 on the gas partial pressure (for $\beta_5 = 0.5$) is

$$i_0 = i_0^0\left(p_{O_2}\right)^{0.875}\left(p_{CO_2}\right)^{-0.25} \quad \text{(A-20)}$$

List of Symbols

F Faraday's number, C·mol^{-1}

i current density, A·m^{-2}

i_0 exchange current density, A·m^{-2}

i_0^0 standard exchange current density, A·m^{-2}

L electrode thickness, m

n number of electrons

p partial pressure, atm

R gas constant, J·mol^{-1}·K^{-1}

S specific surface area, m^{-1}

T temperature, K

x partial pressure dependency of oxygen in MCEC mode

y partial pressure dependency of carbon dioxide in MCEC mode

Greek Letters

α_A anodic transfer coefficient

α_C cathodic transfer coefficient

β symmetry factor

κ_1 effective conductivity of the electrode, S·m^{-1}

κ_2 effective conductivity of the electrolyte, S·m^{-1}

η overpotential, V

References

1 W.H.A. Peelen, K. Hemmes and J. H. W. De Wit, *Electrochim. Acta*, 1997, **43**, 763.

2 V. Kaplan, E. Wachtel, K. Gartsman, Y. Feldman and I. Lubomirsky, *J. Electrochem. Soc.*, 2010, **157**, B552.

3 V. Kaplan, E. Wachtel and I. Lubomirsky, *J. Electrochem. Soc.*, 2012, **159**, E159.

4 D. Chery, V. Albin, V. Lair and M. Cassir, *Int. J. Hydrogen Energy*, 2014, **39**, 12330.

5 L. Hu, I. Rexed, G. Lindbergh and C. Lagergren, *Int. J. Hydrogen Energy*, 2014, **39**, 12323.

6 A. J. Appley and S. Nicholson, *J. Electroanal. Chem.*, 1974, **53**, 105.

7 A. J. Appley and S. Nicholson, *J. Electroanal. Chem.*, 1977, **83**, 309.

8 A. J. Appley and S. Nicholson, *J. Electroanal. Chem.*, 1980, **112**, 71.

9 G. B. Dunks and D. Stelman, *Inorg. Chem.*, 1983, **22**, 2168.

10 M. Takahashi, Extended Abstracts of 21st Symposium on Molten Carbonate Salt Chemistry, Yamanashi, Japan, 1989, p.51.

11 H. R. Kunz, L. J. Bregoli and S. T. Szymanski, *J. Electrochem. Soc.*, 1984, **131**, 2815.

12 R. C. Makkus, H. Hemmes and J. H. W. De Wit, *J. Electrochem. Soc.*, 1994, **141**, 3429.

13 R. C. Makkus, Electrochemical studies on the oxygen reduction and NiO(Li) dissolutionin molten carbonate fuel cells, Ph.D. Thesis, Delft University of Technology, Netherlands, 1991.

14 H. R. Kunz and L. A. Murphy, *J. Electrochem. Soc.*, 1988, **135**, 1124.

15 S. H. Lu and J. R. Selman, *J. Electrochem. Soc.*, 1990, **137**, 1125.

16 W.H.A. Peelen, K. Hemmes and G. Lindbergh, *J. Electrochem. Soc.*, 2000, **147**, 2122.

17 K. Sugiura, K. Takei, K. Tanimoto and Y. Miyazaki, *J. Power Sources*, 2003, **118**, 218.

18 L. Hu, G. Lindbergh and C. Lagergren, To be submitted.

19 C. Lagergren, Electrochemical performance of porous MCFC cathodes, Ph.D. Thesis, KTH Royal Institute of Technology, Sweden, 1997.

20 C. Lagergren and D. Simonsson, *J. Electrochem. Soc.*, 1997, **144**, 3813.

21 L. Plomp and B. J. Veldhuis, *J. Power Sources*, 1992, **39**, 369.

22 C. Lagergren and G. Lindbergh, *Electrochim. Acta*, 1998, **44**, 503.

23 S. Tanase, Y. Miyazaki, M. Yanagida, K. Tanimoto and T. Kodama, *Prog. Batt. Solar Cells*, 1987, **6**, 195.

24 C. Y. Yuh and J. R. Selman, *J. Electrochem. Soc.*, 1991, **138**, 3649.

25 C. Y. Yuh and J. R. Selman, *J. Electrochem. Soc.*, 1991, **138**, 3642.

Figures

Fig. 1 iR-corrected polarization curves for the NiO electrode in electrolysis mode at 650 °C for different gas compositions. (a) O_2, and (b) CO_2.

Fig. 2 iR-corrected polarization curves at low overpotential for the NiO electrode in electrolysis mode for different percentages of O_2. (a) 600 °C, (b) 625 °C, and (c) 650 °C.

Fig. 3 iR-corrected polarization curves at low overpotential for the NiO electrode in electrolysis mode for different percentages of CO_2. (a) 600 °C, (b) 625 °C, and (c) 650 °C.

Fig. 4 Effect of oxygen partial pressure on the exchange current density from 600 to 650 °C.

Fig. 5 Effect of carbon dioxide partial pressure on the exchange current density from 600 to 650 °C.

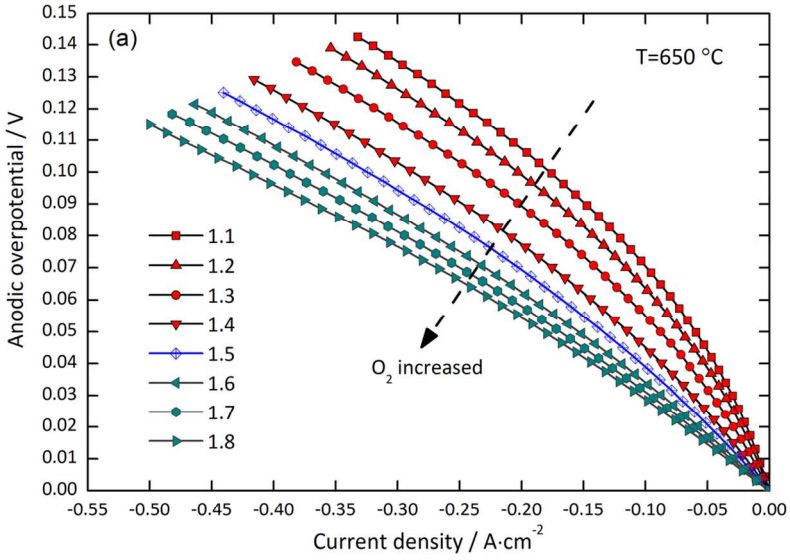

59x40mm (600 x 600 DPI)

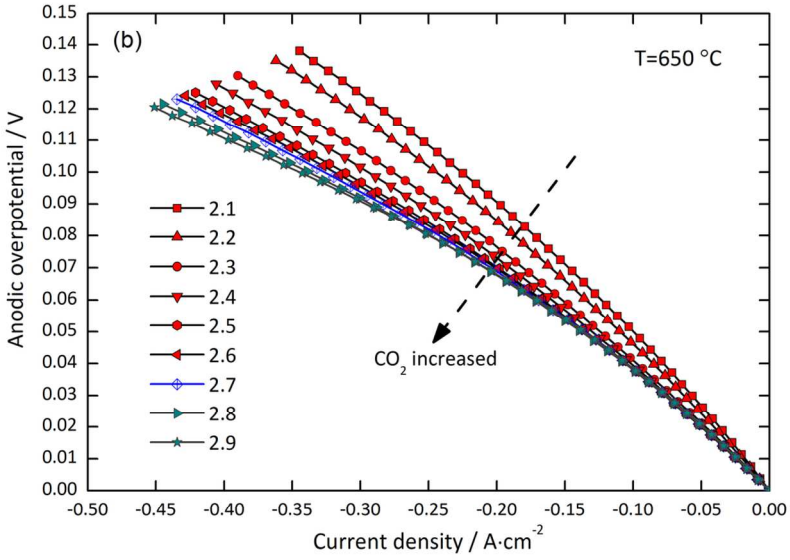

59x40mm (600 x 600 DPI)

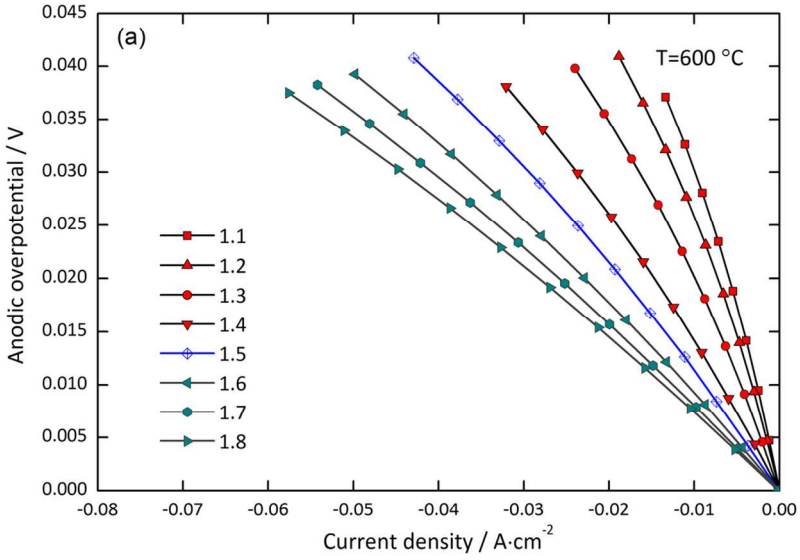

59x40mm (600 x 600 DPI)

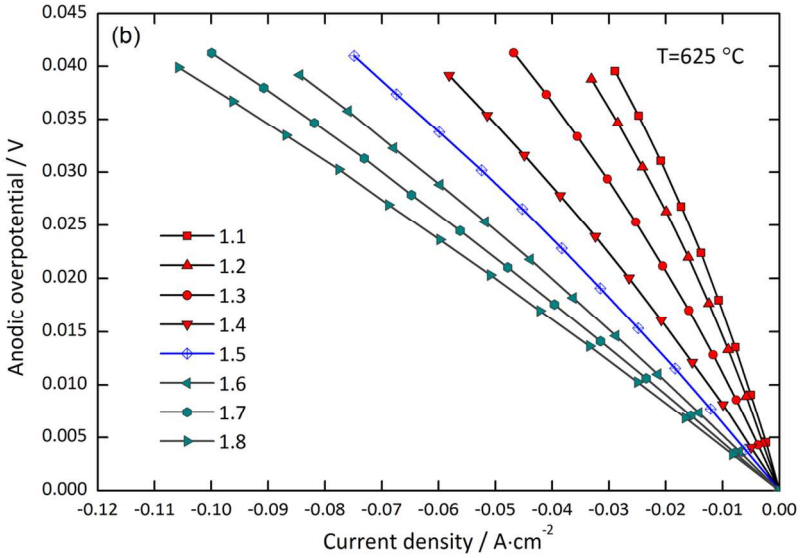

59x40mm (600 x 600 DPI)

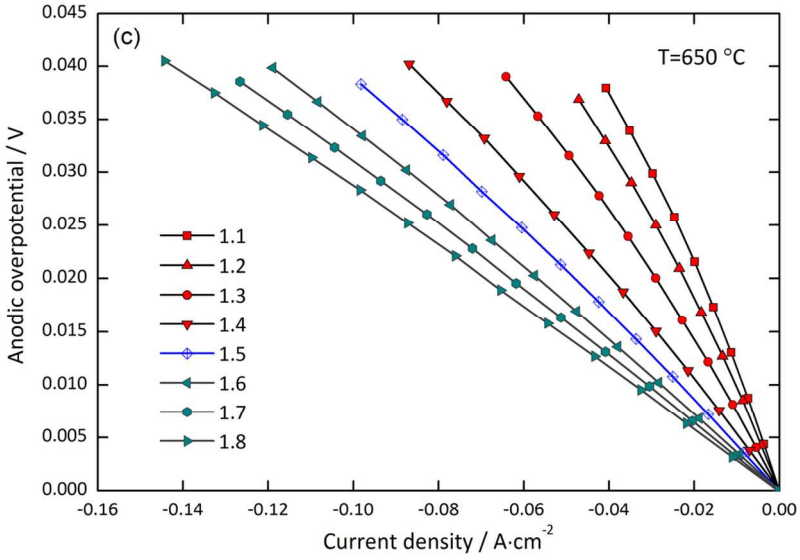

59x40mm (600 x 600 DPI)

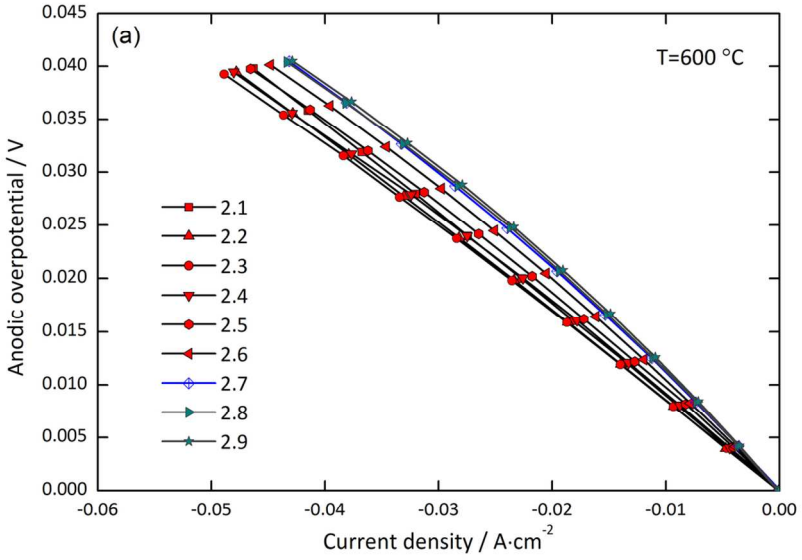

59x40mm (600 x 600 DPI)

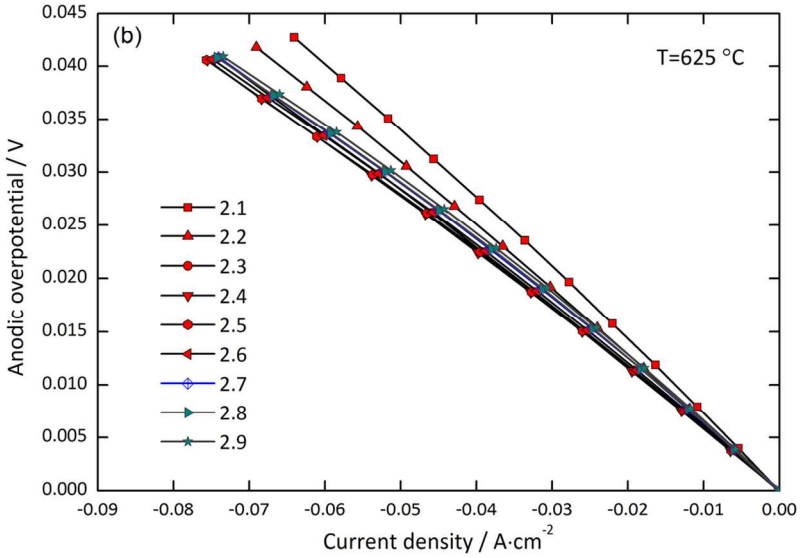

59x40mm (600 x 600 DPI)

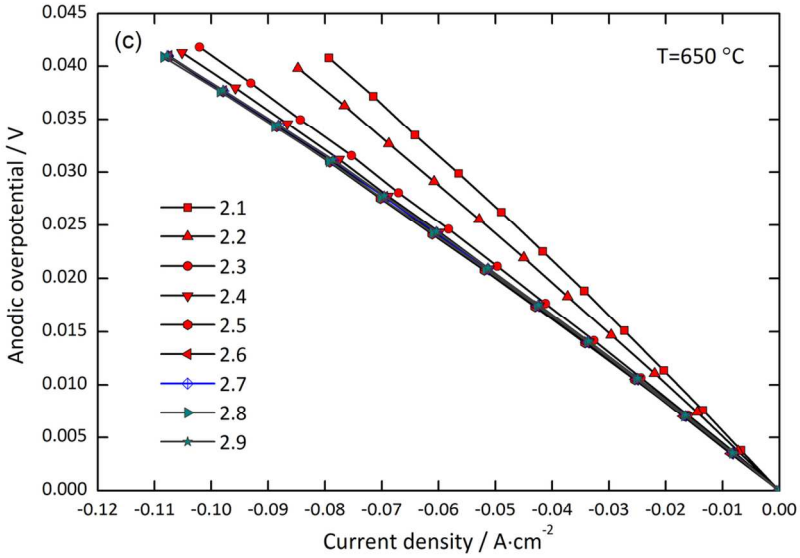

59x40mm (600 x 600 DPI)

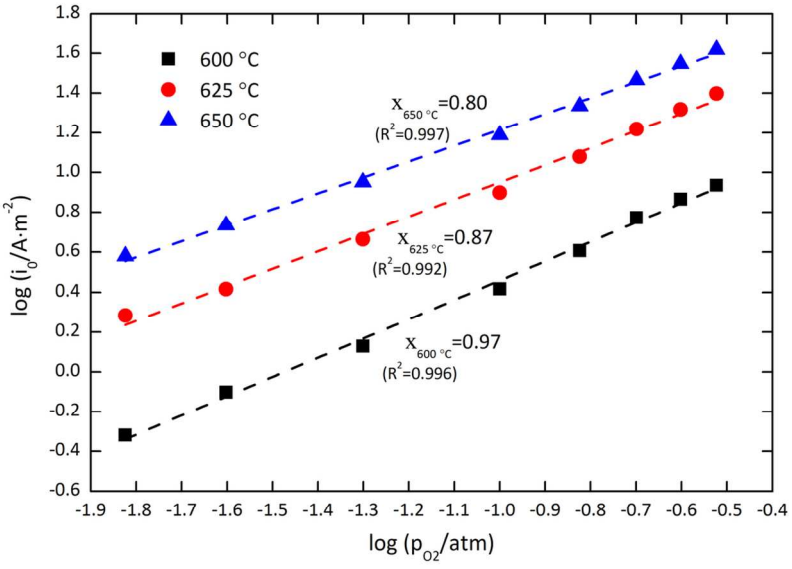

59x40mm (600 x 600 DPI)

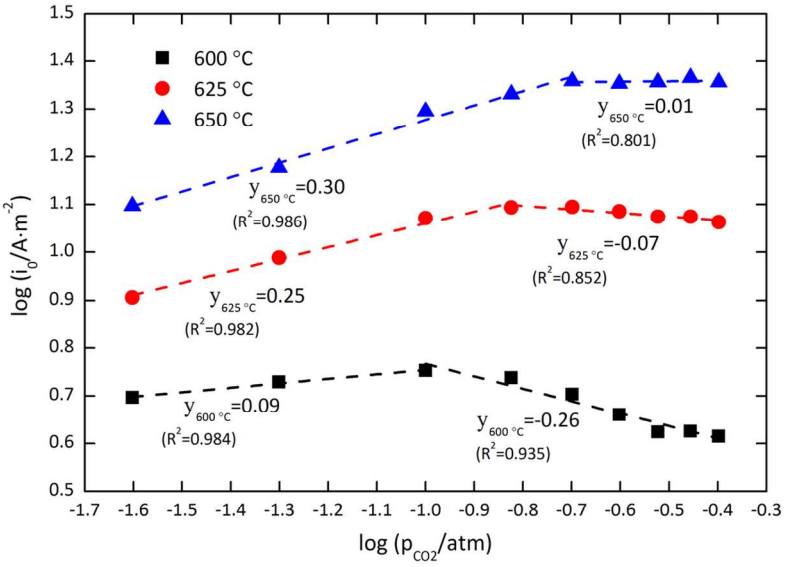

59x40mm (600 x 600 DPI)